Top-down, contextual entrainment of neuronal oscillations in the auditory thalamocortical circuit

Annamaria Barczak[a], Monica Noelle O'Connell[a], Tammy McGinnis[a], Deborah Ross[a], Todd Mowery[b], Arnaud Falchier[a], and Peter Lakatos[a,c,1]

[a]Translational Neuroscience Division, Center for Biomedical Imaging and Neuromodulation, Nathan Kline Institute, Orangeburg, NY 10962; [b]Center for Neural Science, New York University, New York, NY 10003; and [c]Department of Psychiatry, New York University School of Medicine, New York, NY 10016

Edited by Nancy Kopell, Boston University, Boston, MA, and approved July 3, 2018 (received for review August 23, 2017)

Prior studies have shown that repetitive presentation of acoustic stimuli results in an alignment of ongoing neuronal oscillations to the sequence rhythm via oscillatory entrainment by external cues. Our study aimed to explore the neural correlates of the perceptual parsing and grouping of complex repeating auditory patterns that occur based solely on statistical regularities, or context. Human psychophysical studies suggest that the recognition of novel auditory patterns amid a continuous auditory stimulus sequence occurs automatically halfway through the first repetition. We hypothesized that once repeating patterns were detected by the brain, internal rhythms would become entrained, demarcating the temporal structure of these repetitions despite lacking external cues defining pattern on- or offsets. To examine the neural correlates of pattern perception, neuroelectric activity of primary auditory cortex (A1) and thalamic nuclei was recorded while nonhuman primates passively listened to streams of rapidly presented pure tones and bandpass noise bursts. At arbitrary intervals, random acoustic patterns composed of 11 stimuli were repeated five times without any perturbance of the constant stimulus flow. We found significant delta entrainment by these patterns in the A1, medial geniculate body, and medial pulvinar. In A1 and pulvinar, we observed a statistically significant, pattern structure-aligned modulation of neuronal firing that occurred earliest in the pulvinar, supporting the idea that grouping and detecting complex auditory patterns is a top-down, context-driven process. Besides electrophysiological measures, a pattern-related modulation of pupil diameter verified that, like humans, nonhuman primates consciously detect complex repetitive patterns that lack physical boundaries.

auditory perception | oscillations | rhythms | macaque | auditory patterns

Since our auditory environment is composed of a continuous flow of complex, multi-timescale information (e.g., speech/species-specific communication), inputs must be parsed and grouped into meaningful segments to be further processed and interpreted by the brain (1–4). While the mechanisms supporting these processes are not fully understood (5), the repetition of sound sequences or patterns is important for the formation of auditory objects (6). As has been shown in infants, acoustic pattern-repetition recognition is a crucial building block within the language-learning process (7, 8). Recently, Barascud et al. (9) demonstrated that the recognition of novel auditory patterns by adults occurs automatically halfway through the first repetition. Perceptually, repetitive patterns pop out from the ongoing sound sequences despite the absence of a physical boundary defining the start or end of acoustic patterns (9, 10). Concurrent magnetoencephalography (MEG) recordings suggest that the electrophysiological correlate of pattern perception is an increase in tonic activity localized in part to the primary auditory cortex (A1). Still, the details of the circuitry involved in the grouping and parsing of patterns as well as the neuronal dynamics underlying the tonic activity increase in A1 are not yet defined.

Ongoing neuronal oscillations across multiple levels of the auditory pathway can be entrained by repetitive, rhythmically structured auditory stimuli (11–17). Studies of oscillatory entrainment have showed that neuronal oscillations reflect an organized internal state that can be restructured via entrainment to process incoming information efficiently (18, 19). The reorganization of oscillations by sensory stimuli through mechanisms such as phase reset and entrainment has been associated with numerous brain operations, e.g., attention, multisensory integration, and speech perception (20–22). Nevertheless, one could argue that entrainment is purely a reflexive brain response to rhythmically structured inputs related to stimulus onsets and offsets, akin to waves generated by rocking a boat in water. To address this, we explored whether oscillatory entrainment in the A1 occurs in the case of rhythmically repeating auditory patterns that lack physical boundaries and hence are not physically separated from the rest of the sounds in a random continuous "sound cloud" (23). Here, there are no rhythmic acoustic energy fluctuations such as stimulus onsets that could trigger phase reset and entrainment. Only the internal grouping and parsing of the pattern would allow an oscillation to be aligned to the repetitions with a wavelength that matches pattern length.

We hypothesized that patterns, once detected by the brain, would be grouped into rhythmically occurring auditory objects. Neural rhythms could then be aligned via oscillatory entrainment to the structure of the pattern repetitions and aid in parsing and grouping. As opposed to previously demonstrated acoustically driven entrainment of neuronal oscillations (e.g., by rhythmic tone sequences), this form of entrainment depends solely on the brain's ability to group auditory inputs based on their statistical regularities, or context (6, 9), by establishing top-down, internally defined perceptual boundaries—an important process underlying speech learning and perception (3, 4, 24–26). To begin defining the circuitry involved in this process and to distinguish top-down from bottom-up thalamocortical mechanisms,

Significance

Our results indicate that nonhuman primates detect complex repeating acoustic sequences in a continuous auditory stream, which is an important precursor for human speech learning and perception. We demonstrate that oscillatory entrainment, known to support the attentive perception of rhythmic stimulus sequences, can occur for rhythms defined solely by stimulus context rather than physical boundaries. As opposed to acoustically driven entrainment by rhythmic tone sequences demonstrated previously, this form of entrainment relies on the brain's ability to group auditory inputs based on their statistical regularities. The internally initiated, context-driven modulation of excitability in the medial pulvinar prior to A1 supports the notion of top-down entrainment.

Author contributions: P.L. designed research; A.B., M.N.O., T. McGinnis, D.R., and A.F. performed research; T. Mowery contributed new reagents/analytic tools; A.B. and P.L. analyzed data; and A.B. and P.L. wrote the paper.

The authors declare no conflict of interest.

This article is a PNAS Direct Submission.

[1]To whom correspondence should be addressed. Email: Peter.Lakatos@NKI.rfmh.org.

This article contains supporting information online at www.pnas.org/lookup/suppl/doi:10.1073/pnas.1714684115/-/DCSupplemental.

Published online July 23, 2018.

we recorded pattern-related activity in the auditory thalamic relay (the medial geniculate body, MGB) and in a higher-order thalamic nucleus, the medial pulvinar. Importantly, while this study focuses on the A1, MGB, and pulvinar, we do not assume that these are the sole regions involved in auditory pattern recognition and object formation. Our choice of recording sites was based on a decision to sample pattern-related A1 neuronal activity [since pattern-related activity was partially localized here (9)] together with low-level (MGB) and high-level (pulvinar) thalamic structures that are anatomically connected. Moreover, there is some indication that the medial pulvinar may be involved in the parsing of continuous acoustic stimulus sequences such as speech (27–30).

Our results indicate that nonhuman primates' brains can align neuronal oscillations to the temporal structure of repetitive acoustic patterns in the A1, MGB, and medial pulvinar. Phase reorganization in the supragranular A1 coincided with a modulation of multiunit activity (MUA) across cortical laminae, indicating that, similar to bottom-up acoustically driven entrainment, purely top-down context-driven entrainment (31) is also capable of predictive excitability modulation across A1 neuronal ensembles. Interestingly, pattern structure-related excitability modulation occurred earlier in the pulvinar than in the A1 and consisted of MUA suppression at pattern-repeat boundaries. This modulation is theoretically consistent with the parsing or segmentation of the continuous input sequence (32), suggesting that pattern segmentation by the pulvinar or a connected structure is a precursor of contextual entrainment in the A1.

Results

Our study aimed to define the neural correlates of the perceptual parsing and grouping of repeating random tone sequences (patterns) and demonstrate that oscillatory activity can be modulated by internally generated, context-driven cues that lack external acoustic boundaries. To this end, a continuous stream of random sounds, a sound cloud (23), was presented (Fig. 1*A*, *Top*). At random time intervals, 11 sounds were repeated five times (collectively referred to as "pattern repetitions"). In human experiments, this type of stimulus presentation resulted in the perception of five repeating patterns (9). The green asterisk positioned halfway through the first repetition in Fig. 1*A*, Center highlights the time at which Barascud and colleagues found pattern recognition to occur. Importantly, transitions between periods of random and repeating stimuli occurred without any physical change or pause in the stimulus stream. The patterns that emerge at a 1.7-Hz rate (588.5-ms pattern length) are completely defined by context. An examination of the sound cloud amplitude envelope does not reveal their start or end (Fig. 1*A*, *Bottom*), showing that there is no physically detectable boundary or amplitude cue between random and repeating stimuli in the sound cloud. See ref. 33 for a sample sound cloud audio file with one set of pattern repeats.

Since a previous human study (9) localized pattern perception-related neuronal activity in part to the A1, we recorded neuroelectric activity in the A1 together with low-level (MGB) and high-level (medial pulvinar) thalamic structures reciprocally connected to the A1 in four macaques who passively listened to the sound cloud (*Methods*). Data were obtained from a total of 36 A1 and 51 thalamic sites (MGB: $n = 30$; medial pulvinar: $n = 21$). Field potential and MUA profiles were recorded concurrently with linear array multielectrodes. Current source density (CSD) profiles were calculated from field potential profiles. Due to the lack of volume-conducted neuroelectric activity, CSD profiles permit better localization and, in cortex, a more direct physiological interpretation of transmembrane currents underlying sub- and suprathreshold excitability changes in a neuronal ensemble. Fig. 1*B* shows representative auditory click-related CSD and MUA response profiles from each of the targeted areas. Laminar CSD profiles in the A1 show characteristic feed-forward–type activation profiles with an early sink in the granular layer followed by increased amplitude in extragranular layers. Although the MGB and pulvinar lack an apparent laminarly organized structure, and therefore do not satisfy the basic assumptions underlying the application of 1D CSD (34, 35), sinks and sources indexing local net transmembrane current flow can still be observed in CSD profiles. While the interpretation of these sinks and sources is not straightforward, their advantage over field potentials remains, as they reflect strictly local synchronous neuronal events (36).

The "best frequency" (BF) of each cortical and thalamic site was defined as the tone or bandpass noise frequency that evoked the largest MUA response. Fig. 1*C* shows examples of tuning profiles for each of the three recording locations. Determination of the BF was especially important for the A1, since prior studies have indicated that neuronal ensembles tuned to low vs. high frequencies may differ functionally (37, 38). Of the 36 A1 sites sampled, 23 had a BF below 11 kHz, and 13 had a BF equal to or above 11 kHz (Fig. 1*D*).

While the exact hierarchical position of the medial pulvinar in the auditory system is not known, its connectivity throughout the brain is widespread, and it is heavily connected reciprocally to auditory cortical areas (39–45). If the medial pulvinar in the auditory system is positioned similarly to the lateral pulvinar in the visual system, then, hierarchically, the pulvinar could be above the level of primary cortex but still project back to cortical supragranular layers (46–48). Examination of MUA response-onset latencies to auditory clicks support this hierarchical organization within the auditory thalamocortical system: The median MGB, A1, and pulvinar onsets were 3.8, 4.9, and 5.95 ms, respectively. Onsets were significantly different from one another except between those in A1 and pulvinar (Fig. 1*E*).

Entrainment Without Physical Boundaries: Contextual Entrainment. We first examined whether we could replicate the results found by Barascud et al. (9) that showed a significant amplitude increase in the MEG signal localized to the auditory cortex (including the A1) following pattern detection. After calculating the analytic amplitude of the local field potential (LFP), MUA, and CSD signals using the Hilbert transform, our results were opposite those we expected. We found a significant amplitude decrease in A1 activity during pattern repetitions (Fig. 2*A*, boxplots). Although surprising, this finding does not contradict our main hypothesis that, upon the brain's detection of repeating patterns in the sound cloud, the patterns would entrain neuronal oscillations so that they become available for the brain to orchestrate pattern-related perceptual–cognitive operations. While entrainment involves the modulation of the phase and wavelength of ongoing neuronal activity, it does not result in newly added neuronal activity that would lead to an amplitude increase in local recordings (12, 14, 49, 50). Thus, even lacking any amplitude increase, we should find that the phase of delta oscillations at the frequency corresponding to the pattern repetition rate (1.7 Hz) becomes locked to the temporal structure of pattern repetitions around the time when the patterns perceptually emerge in humans (9). Additionally, pattern-related delta oscillatory phase and wavelength alignment, or entrainment, should also result in a pattern-locked delta oscillation that becomes visible in the averaged responses (simulated illustration in Fig. 2*B*). We examined these specific aspects of pattern-related activity next.

To characterize delta phase locking, we calculated pattern-related delta (1.7-Hz) intertrial coherence (ITC), which indexes phase similarity across the 50 repetitive pattern sequences, for all electrode channels and then averaged delta ITC across channels for each A1 site. As the pooled delta ITC waveform and boxplots show (Fig. 2*C*, *Upper*, purple trace and purple boxplots), delta ITC increased significantly during pattern repetitions. After selecting channels with a significant delta ITC peak during pattern repetitions, we found that all 36 A1 sites had at least one channel with significant ITC (mean = 39.2%; SD = 18.5% of all channels per A1 site). ITC for these selected channels (Fig. 2*C*, *Upper*, red trace and red boxplots) reached significance by the third repetition (R3)

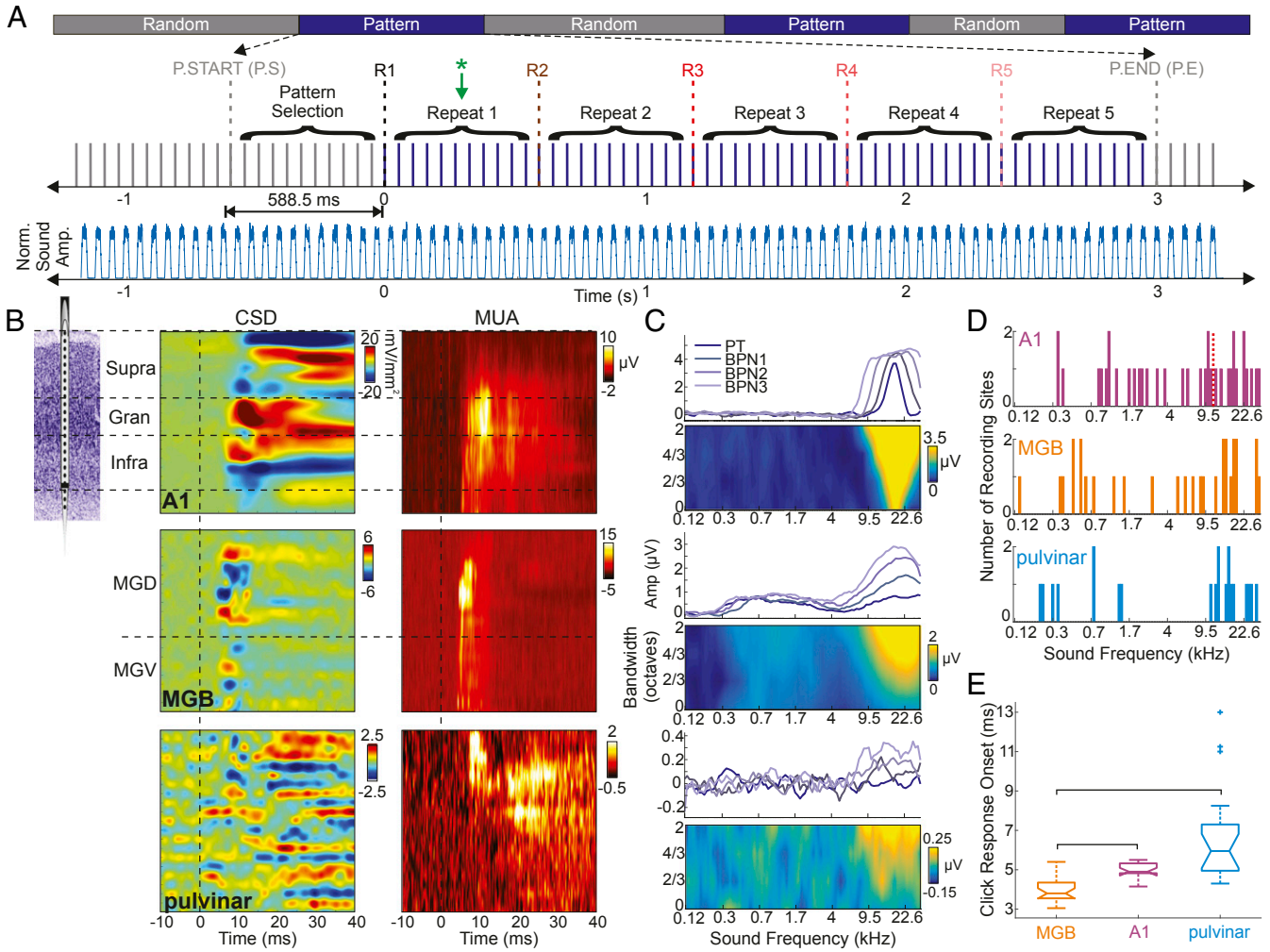

Fig. 1. Auditory paradigm and functional properties of cortical and thalamic areas. (*A*, *Upper*) Pattern-repetition paradigm. The start of the first repetition (R1) is the point at which the pattern becomes theoretically detectable, termed "effective transition" (9), and is designated "0" in all pattern-related plots. (*Lower*) The blue trace is the average analytic amplitude of sounds for 50 patterns from one experiment illustrating that patterns have no physical, acoustically detectable boundaries. (*B*) Schematic of a linear array multielectrode (*Left*) and representative CSD (*Center*) and MUA (*Right*) profiles for recordings in the A1 (*Top*), MGB (*Middle*), and pulvinar (*Bottom*). Transmembrane currents (sinks and sources) in CSD color maps are color-coded red and blue, respectively. Black horizontal dashed lines mark the boundaries of the supragranular, granular, and infragranular layers in the A1 and the approximate border between the dorsal and ventral portions of the MGB. (*C*) Tuning properties of representative A1 (*Top*), MGB (*Middle*), and pulvinar (*Bottom*) recording sites. In each pair the traces show frequency tuning based on averaged MUA responses for pure tones and different bandwidth tone groups. The color maps show the same frequency tuning but with averaged MUA response amplitudes color-coded and mapped on the frequency (*x* axis) and noise bandwidth (*y* axis). (*D*) BFs of all recording sites in the A1 (*Top*), MGB (*Middle*), and pulvinar (*Bottom*) as defined by the frequency of the tone eliciting a maximal-amplitude MUA response. The dashed red vertical line in the *Top* panel marks the BF boundary between low- and high-frequency A1 sites. (*E*) MUA response onsets to auditory clicks pooled across a subset of recording sites from the three locations (MGB, $n = 23$; A1, $n = 16$; pulvinar, $n = 18$). Brackets indicate significant differences between groups, crosses (+ and ‡) denote outliers (Kruskal–Wallis ANOVA with Bonferroni corrected multiple comparisons analysis: H (Kruskal–Wallis ratio) = 34.79, $P = 2.784 \times 10^{-8}$; MGB vs. A1, $P = 0.0003$; MGB vs. pulvinar, $P = 4.1541 \times 10^{-8}$; A1 vs. pulvinar, $P = 0.3732$).

and plateaued around the onset of the fourth repetition (R4), which somewhat matches human performance.

Next, we examined pattern-related delta amplitudes and, despite a general decrease in neuronal activity (Fig. 2*A*), we found an amplitude increase (Fig. 2*C*, *Lower*). We suspected that this amplitude effect was an artifact and did not represent an underlying delta oscillatory process for two reasons. First, the amplitude began to rise at the beginning of pattern selection (P.START) when the brain cannot possibly know that anything will be repeated. Second, the amplitude increase started to decline after R3, which is before the observed ITC peak. This artifact could potentially be due to the reiteration of acoustic patterns that results in the repetition of evoked response patterns and cortical activation at regular intervals biasing our wavelet-based phase and amplitude measures (12, 14, 51). Since the patterns were randomly structured across each stimulus block, response pattern-related phase biases would be random and could only weaken (not contribute to) our ITC findings. However, amplitude changes due to repeating pattern-related responses would always be positive, since repetition at a given wavelength could result in increased amplitude at the corresponding frequency. To verify this, we simulated pattern-related neuronal activity using short (53.5-ms) pieces of averaged CSD responses recorded in A1 sites that showed a significant pattern-related ITC increase. We first averaged responses to each different sound regardless of whether the sound occurred in or outside a pattern repetition and concatenated snippets of these averaged CSD responses in the order in which the stimuli were presented in the original sound cloud. By concatenating responses in the same order, we preserved the individual pattern-related evoked-response structure but eliminated any low-frequency activity related to the

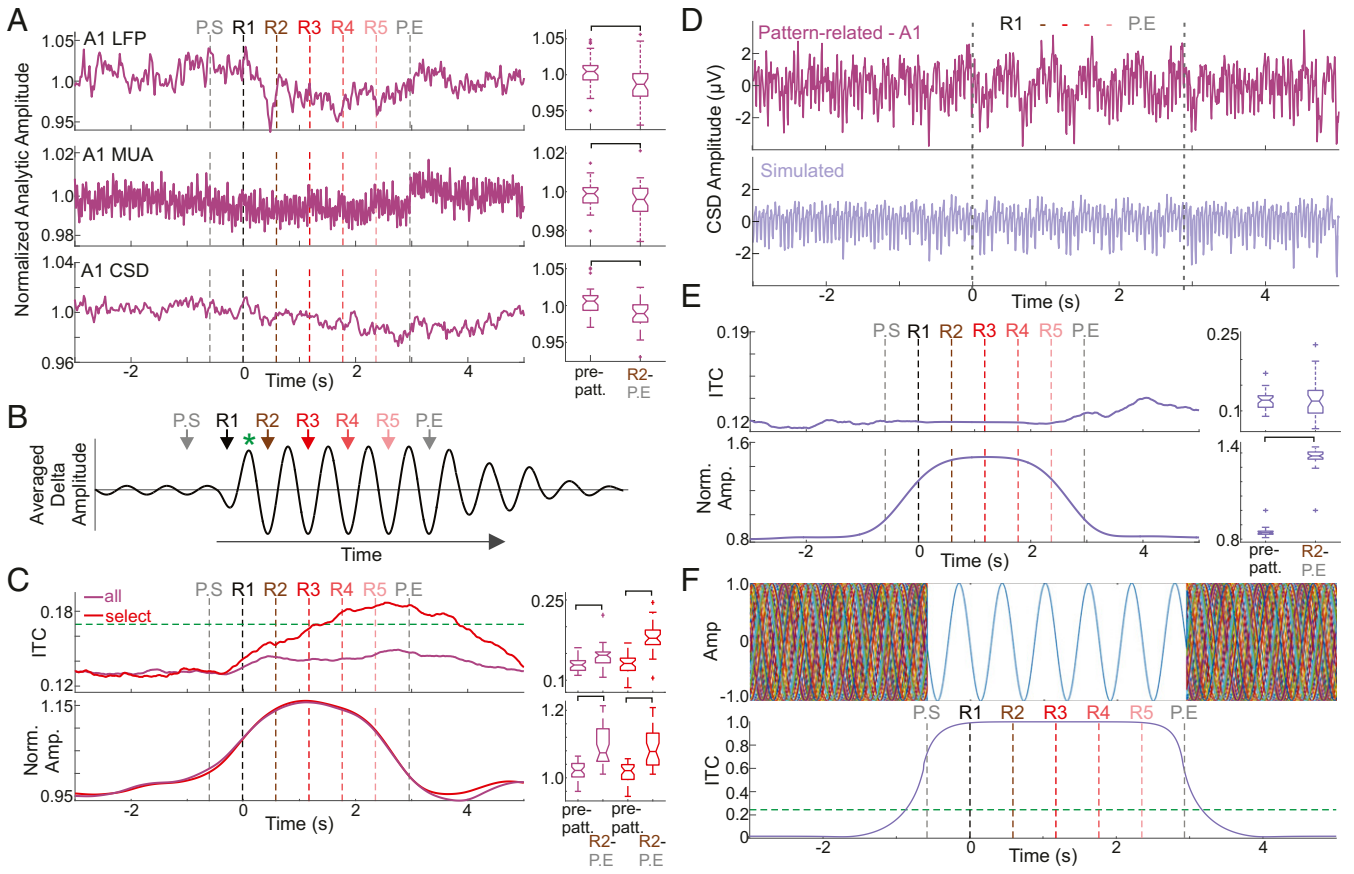

Fig. 2. Pattern-related alignment of neural oscillations in A1. (*A*) Analytic amplitude of pattern-related LFP (*Top*), MUA (*Middle*), and CSD (*Bottom*) averaged across all A1 recordings. Vertical multicolored dashed lines mark the onset of pattern repeats. Boxplots show pooled prepattern (−5,000 to 0 ms) vs. pattern-related (R2–P.END) amplitudes. Brackets indicate a significant difference between periods (Wilcoxon signed rank test, $n = 36$, $P_{LFP} = 0.031$; $P_{MUA} = 0.036$; $P_{CSD} = 0.003$). (*B*) Waveform illustrating our main hypothesis that, despite an amplitude decrease, an oscillation should be visible in the averaged responses if the oscillation is aligned to the temporal structure of pattern repetitions. The green asterisk indicates the approximate time when humans detected patterns (9). (*C*, *Upper*) Traces display pattern-related delta ITC (at 1.7 Hz) averaged across all channels within all A1 sites (purple trace) and across channels in which a significant delta ITC peak (Rayleigh $P < 0.05$) was detected during pattern repetitions (R2–P.END) (red trace). The dashed horizontal line marks the significance threshold as calculated by mean + 2 SD from the baseline ITC across all experiments. Boxplots show that both groups exhibit a significant ITC increase compared with prepattern ITC (Wilcoxon signed rank test, $n = 36$, $P_{ITCall} = 0.0002$; $P_{ITCselect} = 2.35 \times 10^{-7}$). (*Lower*) Traces show delta amplitude for the same two groups as above. Brackets indicate a significant increase of pattern-related delta amplitude (Wilcoxon signed rank test, $n = 36$, $P_{AMPall} = 2.21 \times 10^{-5}$; $P_{AMPselect} = 6.59 \times 10^{-5}$). (*D*) Averaged pattern-related supragranular CSD response from a representative A1 site and the same response simulated. Vertical dashed lines mark the period of pattern repeats. (*E*) As in *C*, but for simulated data. While pattern-related amplitude increase remains significant (Wilcoxon signed rank test, $n = 36$, $P = 6.59 \times 10^{-6}$), there is no pattern-related ITC increase ($n = 36$, $P = 0.86$). (*F*, *Upper*) Simulated data for 50 trials. (*Lower*) The ITC calculated for the 50 simulated trials. The horizontal dashed line signifies the significance threshold ($n = 50$, Rayleigh statistic, $P = 0.05$). P.E., P.END; prepatt., baseline before patterns; P.S., P.START.

pattern repetitions themselves, since low-frequency activity should be random in relation to any given sound onset outside the patterns. Fig. 2*D* shows examples of real and simulated pattern-related supragranular CSD responses and illustrates that, while an apparent delta oscillation is mixed in with the real data (as Fig. 2*B* predicts), this oscillation is missing from the simulated data. After calculating delta ITC and amplitude across all simulated recordings, we found that, while there was a significant delta amplitude increase (Fig. 2*E*, *Lower*), there was no delta ITC increase (Fig. 2*E*, *Upper*), indicating that, as predicted, the amplitude measure is strongly influenced by the pattern of evoked responses. Although evoked responses alone can result in increased delta amplitude, delta ITC indexes a true oscillatory process that disappears within the simulated data.

Finally, to approximate the extent that wavelet analysis-related temporal smearing could impact the timing of our observed ITC, we performed an additional simulation and created 50 trials that consisted of random-phase sinusoidal waves with a frequency of 1.7 Hz ($n = 50$, Rayleigh test of uniformity $P = 0.9743$). For each trial, the signal between P.START and P.END (pattern end) was replaced with a sinusoidal wave of the same phase (Fig. 2*F*, *Upper*) thus exaggerating the impact on ITC of tightly rhythmic activity coinciding exactly with pattern introduction and repetitions. The resulting simulated sine wave-related ITC (Fig. 2*F*, *Lower*) remains significant for 225.5 ms after the end of the last repetition. By comparing this with the timing of significant A1 ITC (Fig. 2*C*, *Upper*), it is evident that A1 ITC remains significant longer than the simulated data. The extended A1 ITC significance beyond pattern cessation and past our simulated signal is a marker of oscillatory entrainment (12, 52) and suggests that pattern-related oscillatory entrainment occurs in the A1.

Pattern-Related MUA Modulation Is Frequency Tuning Specific in the A1. Our ITC measurements indicate that delta oscillatory entrainment occurs during pattern repetitions in A1 recordings. Given that oscillations entrained by rhythmic auditory inputs have been shown to predictably modulate neuronal ensemble excitability across the A1 in a frequency-specific manner (12, 14), we examined whether pattern-related delta oscillations modulate excitability similarly. After selecting the supragranular sink–source electrode

pair with largest amplitudes in auditory-response profiles, we calculated the mean pattern-related phases (during R2–P.END) in each experiment. We used this information to determine whether there was a significant bias in the distribution of mean delta phases across A1 recording sites, which would indicate a preferred phase for entrainment. We found a biased phase distribution (Fig. 3*A*) in the lower supragranular channel (e.g., Fig. 1*B*, red sink in A1 CSD), which corresponds to the active current in auditory responses (12). Since the phase of entrainment has been shown to differ depending on the tuning preferences of A1 neuronal ensembles (37), we also grouped mean phases according to their predetermined BF (Fig. 3*A*, *Middle* and *Lower*) and found that both high- and low-frequency groups showed significant phase bias. A1 sites with a BF <11 kHz ($n = 23$) were entrained to their depolarizing, high-excitability phases, while sites with a BF ≥11 kHz were entrained to their hyperpolarizing phases. The distribution of mean phases across A1 sites tuned to high vs. low frequencies was significantly different (circular Watson–Williams test, $P = 2.72 \times 10^{-5}$) (53, 54) and, as the averaged filtered pattern-related CSD traces show (Fig. 3*B*), were almost opposite.

To directly verify excitability differences at pattern onset, we analyzed the normalized MUA averaged across all layers of the A1 and found significant MUA modulation that largely matched the timing of ITC effects. For A1 sites preferring lower frequencies, MUA was significantly greater at R3, R4, and R5 onsets than MUA measured halfway through each repeat (i.e., 294.5 ms after repeat onset) (Fig. 3*C*, *Upper*), confirming that depolarizing, high-excitability phases of delta oscillations were aligned to repeat onsets. An observed opposite sign effect in high-frequency A1 sites (Fig. 3*C*, *Lower*) provides evidence that delta oscillations are consistently entrained by pattern boundaries in counterphase across A1 regions tuned to low vs. high frequencies. This effect is also implied by the CSD phase distributions (Fig. 3*A*).

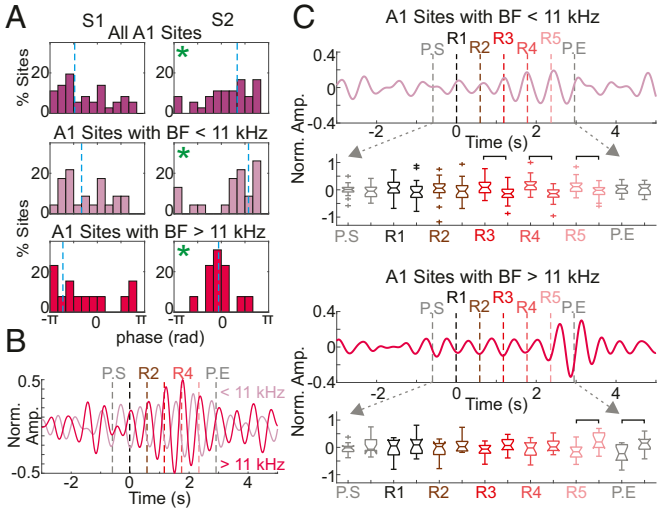

Fig. 3. Pattern-related excitability modulation across differently tuned A1 neuronal ensembles. (*A*) Delta phase distributions for supragranular channels selected based on the largest-amplitude sink–source pair, S1 and S2. Phase distributions for all A1 sites ($n = 36$, *Top*), A1 sites tuned to frequencies <11 kHz (*Middle*), and sites tuned to frequencies ≥11 kHz (*Bottom*). Vertical dashed blue lines indicate mean phases; green asterisks denote significant phase bias as determined by the Rayleigh test of uniformity (all A1 sites: $P_{S1} = 0.20$, $P_{S2} = 0.030$; BF <11 kHz: $P_{S1} = 0.25$, $P_{S2} = 0.002$; BF >11 kHz: $P_{S1} = 0.32$, $P_{S2} = 0.003$). (*B*) Supragranular pattern-related neuronal activity (S2 channels) filtered in the delta band (1.7 Hz ± 20%) and averaged separately across sites according to BF. (*C*) Filtered (1.7 Hz ± 20%), averaged, and normalized MUA averaged across A1 sites with BF <11 kHz (*Upper*) and with BF ≥11 kHz (*Lower*). Boxplots show the distribution of normalized MUA amplitudes at pattern onset and at midway points. Brackets indicate significant MUA amplitude differences (two-sample *t* test, $P < 0.01$).

Pattern Repetition-Related Modulation of Delta Oscillations and Excitability in the Thalamus. Data thus far provide clear evidence that A1 neuronal activity can be aligned to the temporal structure of pattern repetitions in a way that predictively modulates excitability, which likely aids in pattern processing. Next, we wanted to determine if the same was true for the MGB and medial pulvinar. We similarly calculated pattern-related delta ITC and amplitude and found that significant delta ITC occurred in quite a few recording sites across both the MGB and pulvinar (Fig. 4 *A* and *B*, *Upper*; all MGB and pulvinar sites had at least one channel with significant ITC; mean = 35.5%, SD = 15.2% of all channels per MGB site and mean = 35.7%, SD = 15.5% of all channels per pulvinar site). We found no corresponding delta amplitude increase (Fig. 4 *A* and *B*, *Lower*), but the absence of any delta amplitude increase is likely due to the generally lower response amplitudes in the thalamus compared with the A1, which give rise to a much smaller delta amplitude artifact (Fig. 2*E*).

The significantly greater ITC coupled with no significant amplitude change indicates that an oscillation is not added but rather is modulated via oscillatory entrainment to align to the temporal structure of pattern repetitions. As previously stated, entrained oscillations are capable of modulating excitability in a stimulus structure-bound manner. Thus, we looked at MUA amplitudes during pattern repetitions and found that, while no pattern structure-related MUA modulation occurred in MGB (Fig. 4*C*), there was a significant MUA modulation in the pulvinar (Fig. 4*D*). By comparing the boxplots that display MUA amplitude for A1 (Fig. 3*C*) and for pulvinar (Fig. 4*D*), we show that significant differences began to occur in low-frequency A1 sites at R3 (lasting through R5), while in the pulvinar significant modulation began at R1 and (excluding R4) continued for one full repeat after R5 (through P.END). Importantly, pulvinar MUA was significantly suppressed at pattern-repeat onsets. This type of MUA modulation in the pulvinar could reflect a parsing mechanism in which brief inhibitory time periods mark pattern boundaries (32). These results indicate that pattern structure-related excitability modulation occurs earlier in the pulvinar than in the A1 and consists of MUA suppression at pattern-repeat boundaries.

To further characterize timing differences between pattern-related ITC and MUA modulation across the areas examined, we statistically evaluated the onset of significant pattern structure-related ITC and MUA and found no statistical difference in the onset of significant ITC across areas (Fig. 5*A*). Nevertheless, in accordance with our previously described results (Figs. 3*C* and 4*D*), the onset of pattern repetition-related MUA modulation occurred significantly earlier in the pulvinar than in the A1 (Fig. 5*B*). Overall, the earlier modulation of MUA compared with significant pattern-related ITC might indicate that the pattern-related entrainment observed across these areas is the result of MUA modulation.

Although the timing of the MUA amplitude modulation in the pulvinar and A1 indicates a top-down progression of repetitive pattern-related neuronal activity, this does not necessarily mean that the pulvinar plays any role in conveying top-down information about complex auditory patterns to the A1. To examine this, we used pattern-related time-resolved Granger causality (GC) measures in paired pulvinar/A1 recordings ($n = 3$, two monkeys). As Fig. 5*C* shows, pairwise GC increased significantly compared with the baseline (–3,000 to 0 ms) during the R1 in the pulvinar→A1 direction and increased significantly at R4 for the opposite A1→pulvinar direction. This suggests that the pulvinar indeed influences pattern-related A1 neuronal activity and that this influence occurs before the enhanced A1→pulvinar influence.

Conscious Pattern Perception Indexed by Pupil-Diameter Modulation. Observing pattern-related modulation of neuronal activity in A1 and thalamus suggests that, like the human brain, nonhuman primates' brains can detect complex repetitive patterns. However, this does not imply that our subjects consciously perceived

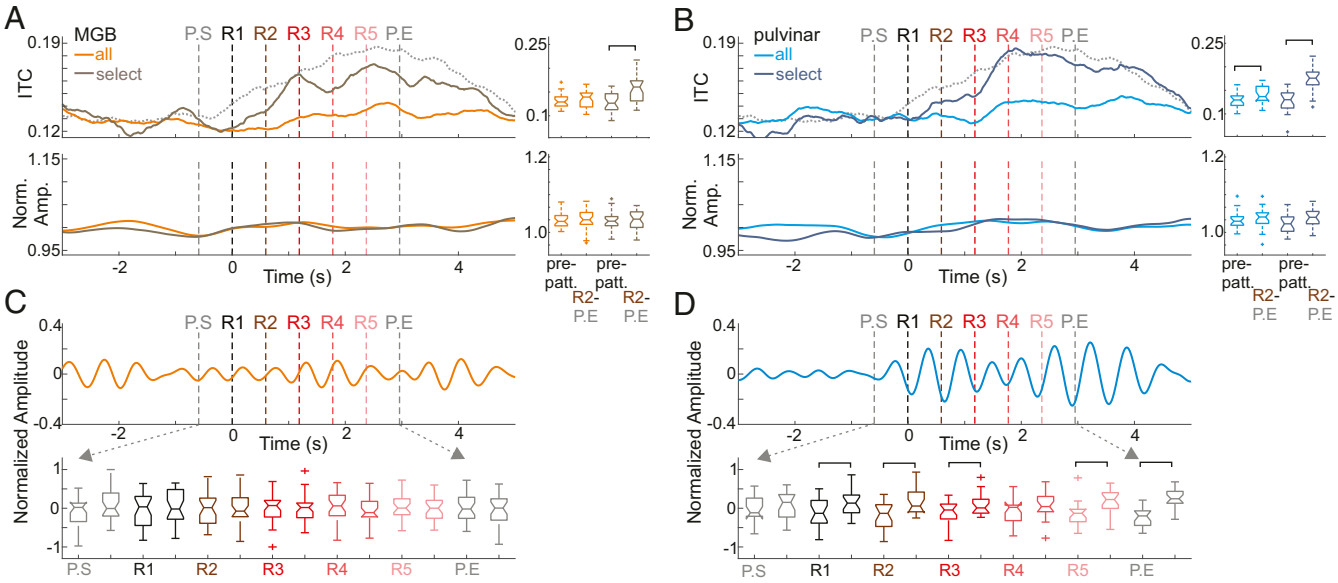

Fig. 4. Delta oscillatory alignment and pattern structure-related excitability modulation in the thalamus. (*A*, *Upper*) Traces display the pattern-related delta ITC averaged across all channels in MGB sites (ITC_{all}, orange) and across channels with a significant delta ITC peak (Rayleigh $P < 0.05$) during the pattern repetitions (ITC_{select}, gold). The gray dashed trace shows ITC measured in significant A1 sites for reference (as in Fig. 2*C*, ITC_{select}). (*Lower*) Traces show the pattern-related data as above but for delta amplitude. Boxplots show that only the select MGB group had a significant ITC increase during patterns (Wilcoxon signed rank test, $n = 30$, $P_{ITCall} = 0.15$; $P_{ITCselect} = 5.7 \times 10^{-5}$). No significant amplitude differences were detected (Wilcoxon signed rank test, $P_{AMPall} = 0.37$; $P_{AMPselect} = 0.55$). (*B*) As in *A*, but for pulvinar recordings. Despite a significant increase in pattern-related ITC for both groups of channels (Wilcoxon signed rank test, $n = 21$, $P_{ITCall} = 0.012$; $P_{ITCselect} = 6.89 \times 10^{-5}$), no significant delta amplitude increase was detected (Wilcoxon signed rank test, $n = 21$, $P_{AMPall} = 0.19$; $P_{AMPselect} = 0.14$). (*C*) Filtered, averaged, and normalized MUA averaged across all MGB sites. Boxplots show the distribution of MUA amplitudes at pattern onset and midway points. (*D*) As in *C* but for pulvinar sites. Brackets indicate significant differences in MUA amplitude (two-sample *t* test, $P < 0.01$).

the patterns. Given that they were not trained to respond to the patterns, we decided to analyze whether, as in humans, changes in pupil diameter could be used to infer whether the patterns were consciously perceived (55). Although our study was not designed to thoroughly analyze pupil dilation modulation, since our subjects were not trained to fixate during pattern presentation, we found a small subset of trials (249 of 8,210 trials) that were devoid of eye movements while gaze was held forward. Traditionally, pupillometry studies mostly examine sustained event-related changes in pupil diameter, so we first determined long-time-scale changes in pupil diameter related to pattern repeats by comparing the unfiltered pupil diameter during patterns with the diameter at baseline immediately prior to the patterns. We found a significant difference between prepattern and pattern-related pupil diameter when measured across trials (Fig. 6*A*), indicative of a conscious perception of pattern repetitions (56).

More recent studies have demonstrated that fluctuations in pupil diameter can occur on timescales that correspond to the delta frequency range of neuronal oscillations and that these fluctuations can even align to music (57, 58). Therefore, we examine whether we could detect any pattern structure-related pupil-diameter effects on this faster timescale. Using the filtered (1.7 Hz ± 20%) pupil signal, we determined whether pupil fluctuations were aligned to patterns by calculating instantaneous phase and ITC during pattern repetitions. When measured across the 249 clean trials, pupil signal-related ITC becomes significant 250 ms after R1 (Fig. 6*B*), which closely matches human behavioral results (9). Additionally, ITC during the prepattern period is statistically smaller than ITC during pattern repetitions. Statistical comparison of oscillatory amplitudes also shows a significant difference during these two periods. Single-trial phases at each pattern-repeat onset are displayed in histograms in Fig. 6*C* and indicate that the mean phases of the pupil signal are biased to a phase just after the negative peak. While this tendency is also observable in the average amplitude of filtered single trials (Fig. 6*D*), the phase bias was significant only at the onset of R2. For comparison, we also performed similar analyses across experiments and with less strict eye movement-selection criteria, which yielded comparable results (*SI Appendix*, Fig. S1).

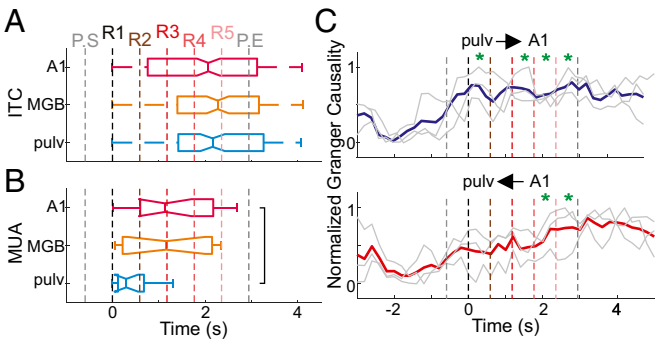

Fig. 5. Summary of ITC and MUA modulation across areas. (*A*) Boxplots show the distribution of time points at which pattern structure-related ITC (at 1.7 Hz) became significant on individual electrode channels ($n = 226$, 134, and 118 for A1, MGB, and pulvinar, respectively). These significant ITC onset distributions were not different from one another (Kruskal–Wallis test, $P_{A1\&MGB} = 0.088$, $P_{A1\&pulv} = 0.262$, $P_{MGB\&pulv} = 0.909$). (*B*) Boxplots show the onsets of significant pattern-related filtered (1.7 Hz ± 20%) MUA. Only experiments with a significant deviation from baseline were included ($n = 19$, 13, 12 for A1, MGB, and pulvinar, respectively). Modulation onsets between A1 and pulvinar were different (Kruskal–Wallis test, $P_{A1\&MGB} = 0.648$, $P_{A1\&pulv} = 0.020$, $P_{MGB\&pulv} = 0.214$). (*C*) Normalized pairwise GC of pattern-related CSD from the pulvinar to the A1 (*Upper*) and from the A1 to the pulvinar (*Lower*). Gray traces show the GC for individual experiments ($n = 3$); colored traces show the average. Asterisks denote pattern repetitions during which the pairwise GC was significantly greater than the baseline (Wilcoxon rank sum test, Bonferroni corrected, pulv→A1: $P_{R1\text{-}R2} = 0.0248$, $P_{R2\text{-}R3} = 0.0562$, $P_{R3\text{-}R4} = 0.0175$, $P_{R4\text{-}R5} = 0.0425$, $P_{R5\text{-}P.END} = 0.0175$; pulv←A1: $P_{R1\text{-}R2} = 0.5449$, $P_{R2\text{-}R3} = 0.2532$, $P_{R3\text{-}R4} = 0.0958$, $P_{R4\text{-}R5} = 0.0237$, $P_{R5\text{-}P.END} = 0.0175$).

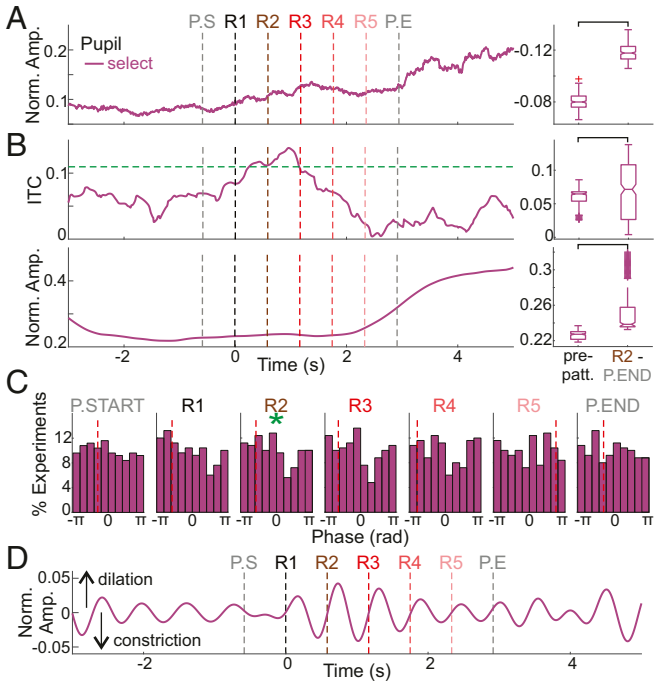

Fig. 6. Pattern-related pupil modulation. (*A*) Normalized unfiltered pupil diameter averaged across clean trials. Boxplots show a significant difference before and during pattern presentation ($n = 249$, Wilcoxon signed rank test, $P = 5.3573 \times 10^{-48}$). (*B*, *Upper*) Traces display pattern-related ITC of the pupil signal averaged across selected trials ($n = 249$). Boxplots show a significant ITC increase ($n = 282$ time points, Wilcoxon signed rank test, $P = 0.0311$). (*Lower*) Traces show normalized delta amplitude for the same trials. Boxplots show a significant difference in amplitude ($n = 282$ time points, Wilcoxon signed rank test, $P = 5.3573 \times 10^{-48}$). (*C*) Single trial phases at pattern-repeat onsets for selected trials. Dashed red vertical lines indicate the mean phase at each pattern repetition. Green asterisks denote significant phase alignment ($n = 249$, Rayleigh test of uniformity, $P_{P.START} = 0.3034$, $P_{R1} = 0.1727$, $P_{R2} = 0.0441$, $P_{R3} = 0.0681$, $P_{R4} = 0.2833$, $P_{R5} = 0.8841$, $P_{P.END} = 0.8831$). (*D*) Normalized delta-filtered pupil diameter averaged across selected trials.

Finally, we performed a time domain analysis similar to that used by Joshi et al. (57). We detected zero crossings of the pupil signal (the time between constriction and dilation when the baseline-corrected pupil signal crosses the 0-amplitude value) in the −3,000-to-0 and R2-to-P.END timeframes. Our results show no difference in the duration ($n = 249$ trials, Wilcoxon signed rank test, $P = 0.1886$) or in the median absolute deviation ($n = 249$ trials, Wilcoxon signed rank test, $P = 0.7371$) of zero crossings before and during pattern presentation. The absence of any difference between these two time periods may be because the experiments used in the cited study were designed to examine pupil-related effects, and our experiments were not. Nonetheless, collectively, these data provide evidence that nonhuman primates' pattern-detection capability and timing is similar to that of humans.

Discussion

Our main aim was to explore the neural correlates of the perceptual parsing and grouping of complex repetitive auditory patterns amid a continuous flow of auditory stimuli. Most importantly, we found that, similar to humans, nonhuman primates have the ability to detect and perceive complex patterns emerging from random sound clouds. Additionally, we demonstrate that entrainment by repetitive rhythmic auditory patterns is possible even when these patterns lack physical boundaries associated with external stimulus parameters/cues. In thalamocortical circuits, auditory patterns are "tracked" by oscillatory activity aligned to the patterns' temporal structure once they are detected. Reorganization of oscillatory activity can then differentially modulate excitability in A1 regions tuned to low vs. high frequencies, like entrainment by simple auditory stimuli and speech (37, 59). While pattern detection by the brain is evidenced by the entrainment of low-frequency oscillations in cortical (A1) and subcortical (MGB and pulvinar) structures, conscious pattern perception in our experiments is indicated by pattern-related modulation of pupil diameter.

Thalamocortical Circuitry of Context-Driven Top-Down Entrainment. Multiple studies have shown that pattern detection is an automatic process and that humans can detect repeating patterns during the first repeat (9, 10, 60). Our findings provide evidence that nonhuman primates' brains can also detect complex repeating patterns embedded in a continuous stream of auditory stimuli. Although our subjects were untrained, pattern repetition-related entrainment of delta activity in the A1 and thalamus occurred with timing like that found in human studies.

The neuronal correlate of pattern detection in humans was shown to be an increase in tonic response amplitude localized to a network of areas that included the A1 (9). Our first goal was to replicate these findings using invasive laminar recordings in the A1. However, the results obtained indicated the opposite: a pattern-related decrease in LFP/CSD amplitude and MUA. The local neuronal dynamics also indicated the alignment of an oscillation to the temporal structure of patterns rather than a tonic response. We believe the discrepancies between the two studies are likely due to differences in the recording methods used. Since MEG is susceptible to volume conduction, synchronous activity across a relatively large region of cortex, such as the auditory cortex, would be detected as an amplitude increase (36, 61). Given that mean oscillatory phases were significantly biased across the neuronal ensembles from which recordings were made (Fig. 3*A*), our results indicate synchrony across at least low-frequency A1 regions. Theoretically, MEG recordings could detect an amplitude increase despite a local amplitude decrease.

Several alternative explanations are worth considering. First, repetitive patterns may be inherently more relevant for humans than for nonhuman primates. In a predictive coding framework, detecting statistical regularities allows the generation of predictions to reduce surprise and, consequently, neural responses. This could explain our reduced-amplitude findings in nonhuman primates, whereas behavioral relevance, which may reverse the effect (62–64), would explain Barascud's findings in humans. Second, Barascud's study utilized a task, while ours did not. At first glance, this difference may seem substantial. However, a portion of the Barascud study also required that human subjects attend to visual stimuli, which rendered the auditory stimuli behaviorally irrelevant. Given that the results obtained in this condition were similar to those obtained when auditory stimuli were relevant, the authors suggest that the process of regularity detection is likely automatic. Since our study did not require subjects to perform a task related to the auditory stimuli, and no rewards were given, our auditory stimuli were also behaviorally irrelevant. Therefore, both sets of results may be indexing the same context-driven, pattern-related synchronization of oscillatory neuronal activity in the A1. Finally, the pattern-related tonic amplitude increase observed in single-channel and rms activity in the Barascud study could reflect a contingent negative variation (CNV)-like activation described in duration timing studies (65, 66) that was not detected by our intracortical recordings.

By examining pattern-related neuronal activity within the MGB and pulvinar, we began to outline the circuitry involved with pattern detection. We hypothesized that context-related entrainment would show a top-down signature, meaning that the pulvinar (a higher-order thalamic nucleus) and the A1, which is connected to the pulvinar with feedback-type projections (39, 40, 67), would align their neuronal activity to the repetitive patterns earlier than the thalamic relay nucleus, the MGB. Our findings that pattern-related MUA modulation occurs earliest in the pulvinar (Fig. 4*D*),

is followed by the A1 (Fig. 3*C*), and is not significant in the MGB (Fig. 4*C*) supports the top-down directionality of events.

The pulvinar's anatomical and physiological properties also suggest that it may be an important part of the circuitry of pattern detection and parsing. The pulvinar is the largest nucleus of the thalamus and has been implicated in numerous cognitive processes (see ref. 68 for a meta-analysis). While the pulvinar's role in auditory-stimulus processing is not completely known, given its association with working memory (69) and its extensive cortical connections (46), the pulvinar may be in an ideal position to coordinate pattern detection across multiple areas that can then assign a relevant (e.g., memory-related, behaviorally relevant) meaning. Since parsing is likely seminal to the chunking of information into meaningful segments, we believe there is growing evidence that corroborates the top-down role of the pulvinar in auditory processing. Several studies show that there is widespread reciprocal connectivity with the language cortex in humans, and there are homologs in monkeys (70–72), while some have specifically suggested that the pulvinar is involved in the parsing of continuous acoustic-stimulus sequences, e.g., speech (27–30). Neuroimaging studies of ultra-fast speech comprehension in blind subjects also implicate the pulvinar in speech segmentation (28, 73). Its role in the parsing of auditory-information streams is also supported by our finding that MUA is suppressed at pattern boundaries (Fig. 4*D*). However, while our study focuses on the possible role of the pulvinar in pattern recognition, other higher-order brain regions likely also contribute to the identification, recognition, and tracking of complex auditory patterns. For example, recent work examining the perception of rhythm (74–76) suggests that the motor system plays a role in the generation of temporal predictions, which may also be important for parsing and tracking auditory patterns.

Pattern-Related Counterphase Modulation of A1 Excitability. Since entrained neuronal oscillations can be utilized to preset the excitability of neuronal ensembles by imposing specific oscillatory phases (12, 14, 77), we asked how pattern-related entrainment modulates excitability in A1 regions tuned to different frequencies. This is especially interesting since our patterns were made up of random tones spanning the monkeys' entire hearing range. In theory these patterns were broadband auditory objects, but, to our surprise, when A1 regions were sorted based on tuning preferences (37), we found an opposite-phase bias. Delta oscillations in sites tuned to lower frequencies were entrained to their high-excitability phases at pattern boundaries, while those in sites tuned to higher frequencies were entrained to their low-excitability phases.

While this differential excitability modulation in A1 regions is clearly demonstrated by the CSD/MUA data in Fig. 3, the functional significance in relation to pattern repetitions is not as clear. We previously hypothesized that low- and high-frequency elements of speech might be processed in counterphase, which would result in a simultaneous opposite-phase entrainment related to click trains across differentially tuned A1 regions (37). Although this notion was recently partially verified (59), an exact mechanistic role of this phenomenon for speech perception is still lacking. One possibility is that oscillations in high-frequency regions provide cyclic inhibition to low-frequency regions, thereby parsing the information contained in the stream of lower-frequency acoustic elements, like the role our results suggest for the pulvinar. The anatomical backdrop for this similarity might be direct medial pulvinar–A1 connectivity, which thus far has been demonstrated only for caudal A1 regions tuned to higher frequencies (78).

Pupil-Indexed Conscious Perception of Auditory Patterns. Auditory stimulus-related pupil-diameter and eye-movement changes have been previously demonstrated in humans. Studies also indicate that the pupil reflects cognitive/perceptual states and can track the temporal structure of stimuli independent of their modality (79, 80). As reviewed by Wang and Munoz (80), physiological cognition-related pupil responses can specify the allocation of attention (58, 82), reflect perceptual selection (83), or indicate the effort being made to listen (84, 85). Pupil-dilation effects have also been used as a proxy for human subjects' reports (55).

Although traditional studies examined pupillary responses in terms of sustained or phasic changes in pupil diameter after a relevant event, a recent study provided evidence that pupil fluctuations are actually quasi-periodic, showing oscillatory patterns in the 1- to 3-Hz frequency range, which corresponds to delta oscillations (57). The quasi-periodic nature of these fluctuations is likely an inherent consequence of the physical structure of the pupil, as the pupil cannot remain dilated at a fixed size forever. Regardless, the frequency of pattern presentation in our study is within the delta frequency range observed by Joshi et al. (57). To fully test the extent to which pupil signals can be modulated based on the frequency of repetitive patterns, further experiments using varying pattern lengths would need to be conducted.

Interestingly, single auditory stimuli can induce a cyclical change in pupil diameter that occurs at about 2 Hz in monkeys and slightly slower in humans (81). Fluctuations of pupil diameter observed in anesthetized cats (86) and in humans (58) have been shown to vary with different types of music, and Kang and Wheatley (58) were able to predict which of two music clips (one played in either ear) subjects were attending to based on the deconvolution of the subjects' pupillary responses. Although there were fluctuations in the loudness of each of the dichotically presented music clips in this latter study, the fluctuations in pupil diameter reflected the attended stream, suggesting that, in addition to stimulus salience, pupillary responses are influenced by higher-level cognitive processes such as attention. Additionally, Ding et al. (87) showed that temporal modulations in music occur predominantly around 2 Hz. Taken together, these results indicate the likelihood of a delta frequency band alignment of pupil-diameter fluctuation to music.

The alignment of pupil-diameter fluctuations to pattern structure observed during repetitive pattern presentation (Fig. 6*B*) in our untrained subjects suggests that pattern recognition in nonhuman primates is an automatic process, as in humans (9). Importantly, the timing of pupil modulation was comparable to the timing of entrainment during the pattern repeats (Figs. 3, 4, and 6) and reinforces the importance and capability of using pupil dilations as covert indicators of perceptual and cognitive processes. These results also indicate that pupil diameter is governed both by automatic and higher-order processes, just like the detection of repetitive patterns in auditory-stimulus sequences.

To summarize, our study provides several converging lines of evidence that demonstrate that entrainment by repetitive rhythmic auditory patterns can occur despite their lacking physical boundaries within a continuous stimulus stream. We have shown that the process of pattern detection, our auditory-object formation, occurs in nonhuman primates' brains with timing comparable to that in humans. We found that pattern-related modulation of neuronal activity occurs first and most robustly in the pulvinar and A1, followed by the MGB, suggesting that the tracking of auditory patterns by neuronal oscillations is orchestrated by a top-down, context-driven process. In addition to electrophysiological evidence for pattern detection, pattern-related modulations of pupil diameter likely reflect conscious pattern perception.

Methods

Subjects. All procedures were approved in advance by the Animal Care and Use Committee of the Nathan Kline Institute. Data from a total of 87 recording sites gathered in 75 experimental sessions with four female macaques (*Macaca mulatta*, 5.0–11.5 kg) obtained from an approved source were used (n = 21, 9, 23, and 22 sessions with macaques T, I, U, and G, respectively).

Eye Tracking. While the macaque's head was immobilized, eye position was monitored at a sampling rate of 120 Hz using the ETL-200 iSCAN Primate Eye Tracking Laboratory (Illumina).

Stimulus Presentation. Subjects passively listened to an auditory-stimulus stream consisting of pure tones and noise bursts with four varying bandwidths (a pure tone, two-thirds of an octave, one and one-third octaves, and two octaves) around center frequencies distributed in the 125–32 kHz frequency range. Roughly 400 different stimuli (97 different center frequencies with four different noise bandwidths) were used and were presented in random order at an 18.7-Hz rate (53.5-ms stimulus onset asynchrony, SOA). At arbitrary time intervals, 11 random sounds were selected from the stream (P.START) and were repeated five times (R1–R5). The pattern length was 588.5 ms (11 × 53.5 ms), corresponding to a 1.7-Hz pattern-repetition rate. Groups of repeating sounds were randomly selected so none of the 50 pattern repetitions within a stimulus block was identical. All sounds were generated using LabVIEW (National Instruments) and were delivered through SA1 stereo amplifiers coupled to MF1 Multi-Field Magnetic Speakers (Tucker-Davis Technologies).

Electrophysiological Recording. Linear array multielectrodes (23 equally spaced contacts) (Fig. 1*B*) were positioned to sample all cortical layers and/or thalamic nuclei simultaneously. Signals were recorded using two PC-based data-acquisition systems: one coupled with LabVIEW (National Instruments) and the other with Alpha Omega SnR software. For additional methodological details, see *SI Appendix, Methods*.

Data Analysis and Signal Processing. To directly compare our data to previously reported human data (9), we downsampled LFP, CSD, and MUA to 1,000 Hz (after rectifying and low-pass filtering the MUA at 300 Hz) and calculated the analytic envelope of each signal using the Hilbert transform. The grand averages of the signal envelopes were compiled by averaging data across all channels within and across A1 sites (Fig. 2*A*). To evaluate pattern-related changes in amplitude, data from the prepattern period (−5,000 to 0 ms) were statistically compared with the pattern-related period (0–2,942.5 ms) using a Wilcoxon signed rank test (Fig. 2*A*, boxplots).

Oscillatory amplitude and phase (Figs. 2–4) were derived from CSD signals transformed to the time–frequency domain using wavelet analysis. Instantaneous power and phase were extracted by wavelet decomposition using the Morlet wavelet (omega = 6) on 54 scales from 0.77 to 21.30 Hz. The wavelet was performed on the continuous data to avoid epoch-related edge effects. Data were then normalized and averaged across targeted events, and the length of the resulting vector was computed. The mean resultant length is also referred to as "intertrial coherence" (ITC) and ranges from 0 to 1 indicating how clustered oscillatory phases are around a mean. Higher ITC values indicate greater clustering, and lower ITC values indicate more random phase distributions. To inspect the influence of evoked-response biases on observed changes in phase and amplitude, we simulated data using averaged CSD response snippets that matched the SOA in length and transformed the simulated data into the time–frequency domain. Delta ITC and amplitude were statistically compared for real and simulated data using Wilcoxon signed rank tests (Fig. 2 *D* and *E*). To examine how a regularly rhythmic signal during pattern repetitions would affect ITC measures temporally, a simulation of 50 trials was created using 50 random-phase sinusoidal waves (1.7-Hz frequency) in which a portion of the sine wave was replaced by a segment with constant phase from P.START to P.END. The simulated sine wave-related ITC was calculated across these 50 trials (Fig. 2*F*).

Entrainment-related effects on excitability (Fig. 3) were determined by pooling the mean phases of all A1 supragranular sink and source pairs. The Rayleigh statistic was used to determine the uniformity of the two phase distributions. Depolarizing, high-excitability phases are located on the downslope of delta oscillations in the CSD of the lower supragranular location, S2 (37, 88). This analysis was repeated after binning A1 recording locations based on their BF. MUA was filtered within a band of ±20% the repetition rate (1.36–2.04 Hz) using a second-order zero-phase-shift Butterworth filter, averaged across all layers within the A1, and normalized to the maximum amplitude. Across each experiment, amplitudes at the onset and midpoint of each pattern repeat were statistically evaluated. Paired comparisons between points of interest were calculated using paired *t* tests. MUA data recorded from MGB and pulvinar sites were analyzed similarly (Fig. 4 *C* and *D*).

Pattern-related significant ITC onsets (Fig. 5*A*) were defined as the time point during repeats at which ITC (at 1.7 Hz) became significant on individual channels. Significant pattern-related MUA modulation onsets (Fig. 5*B*) were calculated using time-resolved *t* tests comparing the amplitude of filtered MUA (averaged across all channels within each recording location) during repeats to that at baseline (−5,000 to 0 ms) across all trials within each experiment. Pooled onsets were statistically compared using a Kruskal–Wallis test followed by a multiple comparisons test using Tukey's honest significant criterion (Fig. 5).

We computed pairwise conditional GC between CSD signals derived from simultaneous linear array multielectrode recordings in the pulvinar and A1 using the MVGC Granger Causality Matlab toolbox by Barnett and Seth (89). Briefly, GC provides a measure of how much the past of a given time series predicts the present of another beyond what is predicted by this other time series' past alone. Before assessing GC, CSD signals were downsampled to 100 Hz. The appropriate vector autoregressive (VAR) model order was calculated automatically based on the Akaike information criterion within the MVGC toolbox. We then checked the stationarity of single trials and excluded those during which the spectral radius of the estimated model was less than 1 (89). Pairwise GC was then calculated using 2,000-ms-wide moving timeframes in 200-ms time steps from −3,000 to 5,000 ms relative to the onset of R1 (Fig. 5*C*).

Only clean pupil signal trials were included in the primary analysis of pupil data. Trials were included if the gaze remained within a 30 × 30° window centered in the monkey's forward-facing visual space and no blinks or large eye movements were made during the −3,000- to 3,000-ms period surrounding each trial onset (R1). To inspect whether pupil size modulation was temporally related to the pattern repetitions (Fig. 6 *B*–*D*), the pupil signal was bandpass filtered (1.7 Hz ± 20%), and instantaneous phase/amplitude was calculated using the Hilbert transform. ITC and normalized amplitude were averaged across trials, and statistical comparisons were calculated using Wilcoxon signed rank tests. Mean pupil phases across pattern repetitions were calculated at the onset of each pattern repeat. Phase distributions were evaluated for significant bias using the Rayleigh statistic (Fig. 6*C*). The delta-band–filtered pupil-diameter trace was normalized by maximum amplitude and averaged across trials (Fig. 6*D*).

Data Availability. The data that support the findings of this study are available from the corresponding author upon reasonable request.

ACKNOWLEDGMENTS. Support for this work was provided by NIH Grants R01DC012947 from the National Institute on Deafness and Other Communication Disorders and R01MH109289 from the National Institute of Mental Health.

1. Buzsáki G (2010) Neural syntax: Cell assemblies, synapsembles, and readers. *Neuron* 68:362–385.
2. Doelling KB, Arnal LH, Ghitza O, Poeppel D (2014) Acoustic landmarks drive delta-theta oscillations to enable speech comprehension by facilitating perceptual parsing. *Neuroimage* 85:761–768.
3. Giraud AL, Poeppel D (2012) Cortical oscillations and speech processing: Emerging computational principles and operations. *Nat Neurosci* 15:511–517.
4. Ding N, Melloni L, Zhang H, Tian X, Poeppel D (2016) Cortical tracking of hierarchical linguistic structures in connected speech. *Nat Neurosci* 19:158–164.
5. Bizley JK, Cohen YE (2013) The what, where and how of auditory-object perception. *Nat Rev Neurosci* 14:693–707.
6. Winkler I, Denham SL, Nelken I (2009) Modeling the auditory scene: Predictive regularity representations and perceptual objects. *Trends Cogn Sci* 13:532–540.
7. Ota M, Skarabela B (2018) Reduplication facilitates early word segmentation. *J Child Lang* 45:204–218.
8. Ota M, Skarabela B (2016) Reduplicated words are easier to learn. *Lang Learn Dev* 12: 380–397.
9. Barascud N, Pearce MT, Griffiths TD, Friston KJ, Chait M (2016) Brain responses in humans reveal ideal observer-like sensitivity to complex acoustic patterns. *Proc Natl Acad Sci USA* 113:E616–E625.
10. Southwell R, et al. (2017) Is predictability salient? A study of attentional capture by auditory patterns. *Philos Trans R Soc B* 372:1–26.
11. Lakatos P, et al. (2016) Global dynamics of selective attention and its lapses in primary auditory cortex. *Nat Neurosci* 19:1707–1717.
12. Lakatos P, et al. (2013) The spectrotemporal filter mechanism of auditory selective attention. *Neuron* 77:750–761.
13. Large EW, Herrera JA, Velasco MJ (2015) Neural networks for beat perception in musical rhythm. *Front Syst Neurosci* 9:159.
14. O'Connell MN, Barczak A, Schroeder CE, Lakatos P (2014) Layer specific sharpening of frequency tuning by selective attention in primary auditory cortex. *J Neurosci* 34: 16496–16508.
15. Simon DM, Wallace MT (2017) Rhythmic modulation of entrained auditory oscillations by visual inputs. *Brain Topogr* 30:565–578.
16. Stefanics G, et al. (2010) Phase entrainment of human delta oscillations can mediate the effects of expectation on reaction speed. *J Neurosci* 30:13578–13585.
17. Zoefel B, Heil P (2013) Detection of near-threshold sounds is independent of EEG phase in common frequency bands. *Front Psychol* 4:262.
18. Buzsáki G, Draguhn A (2004) Neuronal oscillations in cortical networks. *Science* 304: 1926–1929.
19. Schroeder CE, Lakatos P (2009) Low-frequency neuronal oscillations as instruments of sensory selection. *Trends Neurosci* 32:9–18.
20. Lakatos P, Karmos G, Mehta AD, Ulbert I, Schroeder CE (2008) Entrainment of neuronal oscillations as a mechanism of attentional selection. *Science* 320:110–113.

21. Lakatos P, Chen CM, O'Connell MN, Mills A, Schroeder CE (2007) Neuronal oscillations and multisensory interaction in primary auditory cortex. *Neuron* 53:279–292.
22. Ding N, Simon JZ (2012) Emergence of neural encoding of auditory objects while listening to competing speakers. *Proc Natl Acad Sci USA* 109:11854–11859.
23. Mulder MJ, et al. (2013) The speed and accuracy of perceptual decisions in a random-tone pitch task. *Atten Percept Psychophys* 75:1048–1058.
24. Kabdebon C, Pena M, Buiatti M, Dehaene-Lambertz G (2015) Electrophysiological evidence of statistical learning of long-distance dependencies in 8-month-old preterm and full-term infants. *Brain Lang* 148:25–36.
25. Giraud AL, et al. (2007) Endogenous cortical rhythms determine cerebral specialization for speech perception and production. *Neuron* 56:1127–1134.
26. Ghitza O (2011) Linking speech perception and neurophysiology: Speech decoding guided by cascaded oscillators locked to the input rhythm. *Front Psychol* 2:130.
27. Dietrich S, Hertrich I, Ackermann H (2015) Network modeling for functional magnetic resonance imaging (fMRI) signals during ultra-fast speech comprehension in late-blind listeners. *PLoS One* 10:e0132196.
28. Dietrich S, Hertrich I, Ackermann H (2013) Ultra-fast speech comprehension in blind subjects engages primary visual cortex, fusiform gyrus, and pulvinar–A functional magnetic resonance imaging (fMRI) study. *BMC Neurosci* 14:74.
29. Erb J, Henry MJ, Eisner F, Obleser J (2012) Auditory skills and brain morphology predict individual differences in adaptation to degraded speech. *Neuropsychologia* 50:2154–2164.
30. Van Buren JM, Borke RC (1969) Alterations in speech and the pulvinar. A serial section study of cerebrothalamic relationships in cases of acquired speech disorders. *Brain* 92: 255–284.
31. Ghitza O (2016) Acoustic-driven delta rhythms as prosodic markers. *Lang Cognit Neurosci* 32:545–561.
32. von der Malsburg C, Buhmann J (1992) Sensory segmentation with coupled neural oscillators. *Biol Cybern* 67:233–242.
33. Barczak A, et al. (2017) Top-down, contextual entrainment of neuronal oscillations in the auditory thalamocortical circuit [audio recording]. Available at https://osf.io/acpk4/. Accessed August 22, 2017.
34. Nicholson C, Freeman JA (1975) Theory of current source-density analysis and determination of conductivity tensor for anuran cerebellum. *J Neurophysiol* 38:356–368.
35. Mitzdorf U (1985) Current source-density method and application in cat cerebral cortex: Investigation of evoked potentials and EEG phenomena. *Physiol Rev* 65: 37–100.
36. Kajikawa Y, Schroeder CE (2015) Generation of field potentials and modulation of their dynamics through volume integration of cortical activity. *J Neurophysiol* 113: 339–351.
37. O'Connell MN, et al. (2015) Multi-scale entrainment of coupled neuronal oscillations in primary auditory cortex. *Front Hum Neurosci* 9:655.
38. Fishman YI, Reser DH, Arezzo JC, Steinschneider M (2000) Complex tone processing in primary auditory cortex of the awake monkey. II. Pitch versus critical band representation. *J Acoust Soc Am* 108:247–262.
39. de la Mothe LA, Blumell S, Kajikawa Y, Hackett TA (2012) Thalamic connections of auditory cortex in marmoset monkeys: Lateral belt and parabelt regions. *Anat Rec (Hoboken)* 295:822–836.
40. de la Mothe LA, Blumell S, Kajikawa Y, Hackett TA (2006) Thalamic connections of the auditory cortex in marmoset monkeys: Core and medial belt regions. *J Comp Neurol* 496:72–96.
41. Rauschecker JP, Tian B, Pons T, Mishkin M (1997) Serial and parallel processing in rhesus monkey auditory cortex. *J Comp Neurol* 382:89–103.
42. Locke S (1960) The projection of the medial pulvinar of the macaque. *J Comp Neurol* 115:155–169.
43. Ma TP, Lynch JC, Donahoe DK, Attallah H, Rafols JA (1998) Organization of the medial pulvinar nucleus in the macaque. *Anat Rec* 250:220–237.
44. Pandya DN (1995) Anatomy of the auditory cortex. *Rev Neurol (Paris)* 151:486–494.
45. Rosenberg DS, Mauguière F, Catenoix H, Faillenot I, Magnin M (2009) Reciprocal thalamocortical connectivity of the medial pulvinar: A depth stimulation and evoked potential study in human brain. *Cereb Cortex* 19:1462–1473.
46. Shipp S (2003) The functional logic of cortico-pulvinar connections. *Philos Trans R Soc Lond B Biol Sci* 358:1605–1624.
47. Yu C, et al. (2016) Structural and functional connectivity between the lateral posterior-pulvinar complex and primary visual cortex in the ferret. *Eur J Neurosci* 43: 230–244.
48. Zhou H, Schafer RJ, Desimone R (2016) Pulvinar-cortex interactions in vision and attention. *Neuron* 89:209–220.
49. Shah AS, et al. (2004) Neural dynamics and the fundamental mechanisms of event-related brain potentials. *Cereb Cortex* 14:476–483.
50. Makeig S, Debener S, Onton J, Delorme A (2004) Mining event-related brain dynamics. *Trends Cogn Sci* 8:204–210.
51. Zhou H, Melloni L, Poeppel D, Ding N (2016) Interpretations of frequency domain analyses of neural entrainment: Periodicity, fundamental frequency, and harmonics. *Front Hum Neurosci* 10:274.
52. Fiebelkorn IC, et al. (2011) Ready, set, reset: Stimulus-locked periodicity in behavioral performance demonstrates the consequences of cross-sensory phase reset. *J Neurosci* 31:9971–9981.
53. Berens P (2009) CircStat: A MATLAB toolbox for circular statistics. *J Stat Software* 31: 29164.
54. VanRullen R (2016) How to evaluate phase differences between trial groups in ongoing electrophysiological signals. *Front Neurosci* 10:426.
55. Frässle S, Sommer J, Jansen A, Naber M, Einhäuser W (2014) Binocular rivalry: Frontal activity relates to introspection and action but not to perception. *J Neurosci* 34: 1738–1747.
56. Bala AD, Takahashi TT (2000) Pupillary dilation response as an indicator of auditory discrimination in the barn owl. *J Comp Physiol A Neuroethol Sens Neural Behav Physiol* 186:425–434.
57. Joshi S, Li Y, Kalwani RM, Gold JI (2016) Relationships between pupil diameter and neuronal activity in the locus coeruleus, colliculi, and cingulate cortex. *Neuron* 89: 221–234.
58. Kang O, Wheatley T (2015) Pupil dilation patterns reflect the contents of consciousness. *Conscious Cogn* 35:128–135.
59. Zoefel B, Costa-Faidella J, Lakatos P, Schroeder CE, VanRullen R (2017) Characterization of neural entrainment to speech with and without slow spectral energy fluctuations in laminar recordings in monkey A1. *Neuroimage* 150:344–357.
60. Sohoglu E, Chait M (2016) Detecting and representing predictable structure during auditory scene analysis. *eLife* 5:e19113.
61. Lindén H, et al. (2011) Modeling the spatial reach of the LFP. *Neuron* 72:859–872.
62. Kok P, Rahnev D, Jehee JF, Lau HC, de Lange FP (2012) Attention reverses the effect of prediction in silencing sensory signals. *Cereb Cortex* 22:2197–2206.
63. Arnal LH, Giraud AL (2012) Cortical oscillations and sensory predictions. *Trends Cogn Sci* 16:390–398.
64. Summerfield C, Egner T (2009) Expectation (and attention) in visual cognition. *Trends Cogn Sci* 13:403–409.
65. Elbert T, Ulrich R, Rockstroh B, Lutzenberger W (1991) The processing of temporal intervals reflected by CNV-like brain potentials. *Psychophysiology* 28:648–655.
66. N'Diaye K, Ragot R, Garnero L, Pouthas V (2004) What is common to brain activity evoked by the perception of visual and auditory filled durations? A study with MEG and EEG co-recordings. *Brain Res Cogn Brain Res* 21:250–268.
67. Kaas JH, Hackett TA (1998) Subdivisions of auditory cortex and levels of processing in primates. *Audiol Neurotol* 3:73–85.
68. Barron DS, Eickhoff SB, Clos M, Fox PT (2015) Human pulvinar functional organization and connectivity. *Hum Brain Mapp* 36:2417–2431.
69. Arend I, Henik A, Okon-Singer H (2015) Dissociating emotion and attention functions in the pulvinar nucleus of the thalamus. *Neuropsychology* 29:191–196.
70. Hackett TA, Stepniewska I, Kaas JH (1998) Thalamocortical connections of the parabelt auditory cortex in macaque monkeys. *J Comp Neurol* 400:271–286.
71. Ford AA, et al. (2013) Broca's area and its striatal and thalamic connections: A diffusion-MRI tractography study. *Front Neuroanat* 7:8.
72. Morel A, Liu J, Wannier T, Jeanmonod D, Rouiller EM (2005) Divergence and convergence of thalamocortical projections to premotor and supplementary motor cortex: A multiple tracing study in the macaque monkey. *Eur J Neurosci* 21:1007–1029.
73. Dietrich S, Hertrich I, Ackermann H (2013) Training of ultra-fast speech comprehension induces functional reorganization of the central-visual system in late-blind humans. *Front Hum Neurosci* 7:701.
74. Morillon B, Baillet S (2017) Motor origin of temporal predictions in auditory attention. *Proc Natl Acad Sci USA* 114:E8913–E8921.
75. Arnal LH (2012) Predicting "when" using the motor system's beta-band oscillations. *Front Hum Neurosci* 6:225.
76. Fujioka T, Trainor LJ, Large EW, Ross B (2012) Internalized timing of isochronous sounds is represented in neuromagnetic β oscillations. *J Neurosci* 32:1791–1802.
77. Albouy P, Weiss A, Baillet S, Zatorre RJ (2017) Selective entrainment of theta oscillations in the dorsal stream causally enhances auditory working memory performance. *Neuron* 94:193–206.e5.
78. Scott BH, et al. (2017) Thalamic connections of the core auditory cortex and rostral supratemporal plane in the macaque monkey. *J Comp Neurol* 525:3488–3513.
79. Wang CA, Boehnke SE, Itti L, Munoz DP (2014) Transient pupil response is modulated by contrast-based saliency. *J Neurosci* 34:408–417.
80. Joiner WM, Lee JE, Lasker A, Shelhamer M (2007) An internal clock for predictive saccades is established identically by auditory or visual information. *Vision Res* 47: 1645–1654.
81. Wang CA, Munoz DP (2015) A circuit for pupil orienting responses: Implications for cognitive modulation of pupil size. *Curr Opin Neurobiol* 33:134–140.
82. Daniels LB, Nichols DF, Seifert MS, Hock HS (2012) Changes in pupil diameter entrained by cortically initiated changes in attention. *Vis Neurosci* 29:131–142.
83. Einhäuser W, Stout J, Koch C, Carter O (2008) Pupil dilation reflects perceptual selection and predicts subsequent stability in perceptual rivalry. *Proc Natl Acad Sci USA* 105:1704–1709.
84. Zekveld AA, Kramer SE, Festen JM (2010) Pupil response as an indication of effortful listening: The influence of sentence intelligibility. *Ear Hear* 31:480–490.
85. Zekveld AA, Festen JM, Kramer SE (2013) Task difficulty differentially affects two measures of processing load: The pupil response during sentence processing and delayed cued recall of the sentences. *J Speech Lang Hear Res* 56:1156–1165.
86. Mira F, Costa A, Mendes E, Azevedo P, Carreira LM (2016) Influence of music and its genres on respiratory rate and pupil diameter variations in cats under general anaesthesia: Contribution to promoting patient safety. *J Feline Med Surg* 18:150–159.
87. Ding N, et al. (2017) Temporal modulations in speech and music. *Neurosci Biobehav Rev* 81:181–187.
88. Lakatos P, et al. (2005) An oscillatory hierarchy controlling neuronal excitability and stimulus processing in the auditory cortex. *J Neurophysiol* 94:1904–1911.
89. Barnett L, Seth AK (2014) The MVGC multivariate Granger causality toolbox: A new approach to Granger-causal inference. *J Neurosci Methods* 223:50–68.